Fibroblast Growth Factor Receptors Control Epithelial–Mesenchymal Interactions Necessary for Alveolar Elastogenesis

Sorachai Srisuma[1,2,3], Soumyaroop Bhattacharya[1,3], Dawn M. Simon[3,4], Siva K. Solleti[1], Shivraj Tyagi[3], Barry Starcher[5], and Thomas J. Mariani[1,3]

[1]Division of Neonatology and Center for Pediatric Biomedical Research, Department of Pediatrics, University of Rochester Medical Center, Rochester, New York; [2]Department of Physiology, Faculty of Medicine Siriraj Hospital, Mahidol University, Bangkok, Thailand; [3]Department of Medicine, Brigham and Women's Hospital, Harvard Medical School, Boston, Massachusetts; [4]Division of Pulmonology, Allergy/Immunology, Cystic Fibrosis, and Sleep, Department of Pediatrics, School of Medicine, The Emory-Children's Center, Atlanta, Georgia; and [5]Department of Biochemistry, University of Texas Health Center, Tyler, Texas

***Rationale*: The mechanisms contributing to alveolar formation are poorly understood. A better understanding of these processes will improve efforts to ameliorate lung disease of the newborn and promote alveolar repair in the adult. Previous studies have identified impaired alveogenesis in mice bearing compound mutations of fibroblast growth factor (FGF) receptors (FGFRs) 3 and 4, indicating that these receptors cooperatively promote postnatal alveolar formation.**

***Objectives*: To determine the molecular and cellular mechanisms of FGF-mediated alveolar formation.**

***Methods*: Compound FGFR3/FGFR4-deficient mice were assessed for temporal changes in lung growth, airspace morphometry, and genome-wide expression. Observed gene expression changes were validated using quantitative real-time RT-PCR, tissue biochemistry, histochemistry, and ELISA. Autocrine and paracrine regulatory mechanisms were investigated using isolated lung mesenchymal cells and type II pneumocytes.**

***Measurements and Main Results*: Quantitative analysis of airspace ontogeny confirmed a failure of secondary crest elongation in compound mutant mice. Genome-wide expression profiling identified molecular alterations in these mice involving aberrant expression of numerous extracellular matrix molecules. Biochemical and histochemical analysis confirmed changes in elastic fiber gene expression resulted in temporal increases in elastin deposition with the loss of typical spatial restriction. No abnormalities in elastic fiber gene expression were observed in isolated mesenchymal cells, indicating that abnormal elastogenesis in compound mutant mice is not cell autonomous. Increased expression of paracrine factors, including insulin-like growth factor−1, in freshly-isolated type II pneumocytes indicated that these cells contribute to the observed pathology.**

***Conclusions*: Epithelial/mesenchymal signaling mechanisms appear to contribute to FGFR-dependent alveolar elastogenesis and proper airspace formation.**

Keywords: lung development; fibroblast growth factor receptor; alveogenesis; insulin-like growth factor−1; microarray

AT A GLANCE COMMENTARY

Scientific Knowledge on the Subject

The mechanisms contributing to formation of the alveolus are poorly understood. Prior studies indicate a cooperative role for fibroblast growth factor receptor (FGFR)-3 and FGFR-4 in alveolar formation. The temporal, cellular, and molecular nature of the mechanism(s) involved have not been fully elucidated.

What This Study Adds to the Field

We demonstrate that epithelial–mesenchymal paracrine signaling contributes to the regulation of alveolar elastic fiber formation.

Lung development is regulated by finely orchestrated processes of molecular events that determine the temporal and spatial formation of structures that become a fully functional respiratory apparatus. The final stage of lung maturation involving the formation of alveoli, or alveogenesis, is defined by secondary crest septation from primary walls of primitive airspace saccules. These septae subdivide the saccules into mature alveoli, resulting in an enlarged respiratory surface area for gas exchange. Alveogenesis begins at about 32 weeks of gestation in humans, and alveoli continue to form for up to 8 years postnatally (1–4). In mice, this process occurs entirely after birth, initiating at the end of the first week of life and continuing for up to 1 month. Disruption of this physiological process results in incomplete lung maturation, with insufficient gas exchange as evidenced by morbidity of prematurity. Furthermore, impairment of lung formation or abnormal repair after lung injury can lead to the loss of functional terminal airspace, which is associated with several chronic lung diseases, including bronchopulmonary dysplasia in children and emphysema in adults. Many chronic lung diseases could benefit from therapeutic approaches aimed at promoting the process of alveogenesis to increase lung function. However, our current lack of a thorough understanding of the mechanisms controlling lung maturation, maintenance, and repair limits the therapeutic approaches to combat lung disease.

Disruption of connective tissue fiber assembly has been implicated as one mechanism of abnormal airspace dilatation and attenuated alveolar septal formation (5). Early-onset pulmonary emphysema has been observed in some monogenic diseases involving extracellular matrix (ECM) genes, including Cutis laxa secondary to mutations in the genes encoding elastic

(*Received in original form April 9, 2009; accepted in final form January 20, 2010*)

Supported by National Heart, Lung, and Blood Institute contract grant HL071885 (T.J.M.).

Correspondence and requests for reprints should be addressed to Thomas J. Mariani, Ph.D., Division of Neonatology and Center for Pediatric Biomedical Research, University of Rochester, 601 Elmwood Avenue, Box 850, Rochester, NY 14642. E-mail: tom_mariani@urmc.rochester.edu

This article has an online supplement, which is accessible from this issue's table of contents at www.atsjournals.org

Am J Respir Crit Care Med Vol 181. pp 838–850, 2010
Originally Published in Press as DOI: 10.1164/rccm.200904-0544OC on January 28, 2010
Internet address: www.atsjournals.org

fiber components tropoelastin (6) and fibulin-5 (7), Marfan syndrome from mutations in the gene encoding the elastic fiber component fibrillin-1 (8), and Ehlers-Danlos syndrome from mutation in the gene encoding collagen (COL3A1) (9). Similarly, disruption in connective tissue formation during the neonatal period due to prematurity, barotrauma, volutrauma, long-term oxygen exposure, corticosteroid exposure, or infection impacts the developing lung and compromises alveolar maturation, which may predispose to the development of chronic lung diseases (10).

Elastic fibers are complex structures that uniquely confer the property of recoil to mammalian tissues, including the vasculature, skin, and lung. Elastic fibers are composed predominantly (~90%) of an insoluble polymer of tropoelastin molecules, complexed to a number of protein and proteoglycan components, including members of the fibrillin, fibulin, and latent transforming growth factor (TGF) binding protein families (11). A number of rodent models have demonstrated primary postnatal alveolar septal defects associated with disruption of ECM assembly in the lung, particularly associated with elastic fiber formation. Mice lacking tropoelastin exhibit severe lung development defects (12). Neptune and colleagues (13) reported that excessive TGF-β1 is the cause of developmental airspace enlargement in fibrillin-1 hypomorphic mice. Mice bearing deletion of platelet-derived growth factor–α (14) or compound mutations of retinoid receptors (RXR-α and RAR-γ) (15) display a significant reduction of lung elastic fiber content associated with reduced alveolar formation. Interestingly, all of these studies illustrate the critical role for ECM assembly and remodeling upon alveolar formation.

Fibroblast growth factor (FGF) signaling is critical for multiple stages and processes during lung development including alveogenesis. Increased expression of FGF receptors (FGFRs) 3 and 4 coincides with alveolar formation (16). Reduced expression of FGFR3 (17) and FGFR4 (18) is associated with reduced alveolar formation in rat lung neonates after hyperoxic injury. Failure of alveogenesis has been shown in mice deficient in both FGFR3 and FGFR4, but not deletion of either receptor alone (19). However, little is known about the mechanisms for FGFR regulation of alveogenesis.

In microarray data describing normal murine lung development, we previously showed that FGFR3 and FGFR4 cocluster with a group of ECM molecules, including molecules contributing to basement membrane and elastic fiber formation (20, 21). Several studies have demonstrated that FGFR signaling contributes to the regulation of ECM expression and composition (22, 23). We hypothesized that FGFR signaling contributes to the control of ECM formation, which is essential for alveogenesis. In this study, we confirmed the combined necessity of FGFR3 and FGFR4 for alveogenesis in the inbred C57BL/6 mouse lung, and defined the contribution of FGF signaling to the regulation of alveogenesis using gene expression profiling. We demonstrate that excessive elastic fiber gene expression in FGFR3/4 mutant lungs is associated with primary abnormalities in type II pneumocyte (AT2) phenotype resulting in defective epithelial–mesenchymal interactions coordinating alveolar morphogenesis. Some of the results of these studies have been previously reported in the form of abstracts (24–26).

METHODS

Animals

Animal experimentation protocols for this study were reviewed and approved by the Institutional Animal Care and Use Committee at Harvard Medical School, and were conducted following national guidelines for the care and protection of animals. All animals were maintained in a pathogen-free barrier facility.

Generation of FGFR3 and FGFR4 Compound Homozygous and Heterozygous Mice

Mice heterozygous for targeted disruption of FGFR3 were obtained from Dr. David Ornitz (Washington University, St. Louis, MO) (27). FGFR4 heterozygote mice were obtained from Chu-Xia Deng (National Institute of Diabetes and Digestive and Kidney Diseases, National Institutes of Health, Bethesda, MD) (19). All animals were bred to and maintained in a pure C57BL/6 background. FGFR4 heterozygotes were bred with FGFR3 heterozygotes to generate compound heterozygotes. The compound heterozygotes were then intercrossed to generate FGFR3 heterozygote and FGFR4 mutant mice. The double-mutant animals were generated by interbreeding FGFR3 heterozygote and FGFR4 mutant mice. Results are reported for wild-type, compound heterozygous and compound mutant mice. All other intermediate genotypes were screened for preliminary analysis. Genotyping was performed by PCR analysis as described previously for FGFR3 (28) and FGFR4 gene disruption (19).

Lung Histology

After mice were killed, a cannula was inserted into the trachea and secured with 4–0 suture (Roboz Surgical, Gaithersburg, MD). The lungs were exposed, and pulmonary vasculature was perfused with phosphate-buffered saline (PBS). The right lung was sutured, resected, and flash frozen in liquid nitrogen for RNA and protein isolation. The left lung was inflated via tracheal cannula to a fixed pressure of 25 cm H_2O with 10% buffered formalin for 15 minutes. At the end of the fixation period, the trachea was ligated, and heart and inflated lung were removed *en bloc* and immersed in 30 ml 10% buffered formalin for 48 hours at room temperature. After fixation and heart removal, the lung was sectioned midsagitally and embedded in paraffin for histological and morphological analysis. Sections (5-μm thick) were cut with a microtome and stained with hematoxylin and eosin.

Lung Morphometry

Quantitative assessment of lung structure was performed essentially as we have previously published (29). The slides were stained with a modified Gill's hematoxylin (100 ml Harris hematoxylin and 100 ml Gill's No. 3 hematoxylin [Sigma, St. Louis, MO]) overnight at room temperature. The slides were then washed and treated in dilute ammonium hydroxide for 5 minutes, then dehydrated through gradient ethanol and washed in xylene. Ten random, high-powered fields were captured from each slide chosen for morphometry using Leica QWin image software (Leica Microsystems, Wetslar, Germany). These images were then analyzed with Scion Image (Scion Corp., Frederick, MD) to determine the linear distance between alveolar walls (chord length) and the size of individual airspaces (airspace size). Briefly, at least 10 nonoverlapping fields (at 200× original magnification) were analyzed per animal. A threshold function was used to digitally differentiate tissue elements representing airspace walls and the airspaces they bound. Poorly inflated regions and regions containing conducting airways, vasculature, and pleura were avoided. To reduce optical and histological processing noise, and for comparison with previous studies, chords smaller than 8 and greater than 250 μm were excluded (30). All discontinuous airspaces (including saccules, alveoli, and alveolar ducts) completely bounded by tissue elements, irrespective of size and shape, were identified. The area was calculated as the number of pixels contained in each airspace multiplied by a normalization factor (pixels/μm). Individual area measurements less than 25 μm^2 were excluded, as they clearly represented artifacts. The mean chord length and airspace size was then calculated for each animal for comparison among genotypes.

Oligonucleotide Microarray Experiments

Total RNA was prepared from whole lung tissue ($n = 9$ lungs for each age–genotype group) using TRIzol reagent (Invitrogen, Carlsbad, CA). DNA-free RNA (10 μm) for three lungs were pooled (by age and genotype) and repurified using the RNeasy Mini Kit (Qiagen, Valencia, CA). Targets from pooled RNA samples ($n = 3$ pools for each age–genotype group) were generated as described previously (31), and hybridized to Mouse Expression Array 430 2.0 (Affymetrix, Santa Clara, CA).

All arrays passed strict quality control criteria. Expression intensities were obtained from the .CEL files using three different extraction methods: Robust Multichip Average–generated normalized background-subtracted data; DNA Chip analyzer (32) normalized data; and Microarray Suite 5.0 nonnormalized background-subtracted data. All the above algorithms were implemented using BioConductor (http://www.bioconductor.org/). Each of these datasets was subjected to nonparametric bootstrap analysis using MultiExperimental Viewer 3.0 (Dana-Farber Cancer Institute, Boston, MA) to detect the underlying association among the samples (http://www.tm4.org/mev.html).

Differential expression between compound heterozygotes and compound mutant samples was assessed by two independent tests using MultiExperimental Viewer 3.0; the Student's *t* test and Significant Analysis of Microarray (SAM) (33). Each test was applied to the three versions of data, providing a total of six comparisons. Differential expression for selected probe sets was analyzed using the Affymetrix Difference Call algorithm, from GeneChip Operating Software (GCOS) 1.2 (Affymetrix) for each of the pair-wise comparisons. Annotation information of probe sets was retrieved from the Affymetrix analysis portal (http://www.netaffx.com/).

Quantitative Real-Time RT-PCR

Reverse transcription was performed using oligo dT primers and MultiScribe reverse transcriptase (Applied Biosystems, Foster City, CA). Quantitative real-time RT-PCR (qPCR) was performed in triplicate for each sample, as described previously (29), using SYBR green chemistry (Applied Biosystems) on an Mx3000P real-time PCR system (Stratagene, La Jolla, CA). qPCR assays were performed for the selected genes in each sample (n = 7–12 lungs each age–genotype group; n = 5–7 experiments of isolated cells per each genotype). The expression level of each gene in each sample was normalized to the level for the endogenous control cyclophilin A (PPIA), or surfactant protein (SP)–C for isolated AT2, and calculated using the mean of difference in cycle threshold in the mutant samples from the cycle threshold for the controls (age-matched wild types or compound heterozygotes) as a calibrator. The value of a calibrator was calculated as the mean of the difference in cycle threshold for all age-matched control samples. The mean expression for compound mutants was calculated as a fraction of that for controls for individual experiments.

Histochemical Staining for Elastic Fibers

Lung sections were deparaffinized, hydrated, and then stained with resorcin–fuchsin solution overnight at room temperature, according to modified Hart's methods (34, 35). After being washed in water, sections were counterstained with tartrazine, dehydrated in ethanol, cleared in xylene, and mounted. Elastic fibers are visible in purple with yellow counterstain. A minimum of six animals were assessed in each age–genotype group.

Quantification of Lung Elastin Content

Elastin content was determined using a radioimmunoassay for desmosine, as previously described (36).

Immunohistochemistry/Cytochemistry

Immunostaining was performed essentially as previously described (37, 38). SP-C goat polyclonal IgG antibody (400 ng/ml; Santa Cruz Biotechnology, Santa Cruz, CA) was used to detect SP-C. Mouse monoclonal alkaline phosphatase–conjugated antibody (400 ng/ml; Sigma) was used to detect α–smooth muscle actin (αSMA). Monoclonal rat anti-mouse IgG antibody (19 μg/ml; Dako, Glostrup, Denmark) was used to detect Ki67. The frequency of stained cells was defined by manually counting the number of Ki76-stained cells, and automated counting of the total number of nuclei per high power field.

Isolation of Murine Alveolar Type II Epithelial and Lung Mesenchymal Cells

Mouse alveolar type II epithelial and lung mesenchymal cells from 3-week-old C57BL/6 wild-type and FGFR3/4 compound mutant mice were isolated essentially as described previously (39) with minor modifications. Briefly, the lungs were perfused with 5–10 ml of PBS injected through the right ventricle. Dispase (1 ml; Roche Applied Science, Indianapolis, IN) was instilled into the lungs with a 3-ml syringe attached to a 20-gauge luer stub adapter (BD Biosciences, Bedford, MA) through the trachea. Next, 0.5 ml of 1% low-melting agarose (Invitrogen) was instilled into the lungs, and the trachea was sutured to avoid the leakage of dispase and agarose. The heart–lung blocs were dissected; the heart, thymus, and trachea were removed. The lungs were removed to a sterile tube with 2 ml of dispase enzyme and incubated at room temperature for 45 minutes for enzymatic digestion. Lung tissue was separated from the main airways and teased apart in 3 ml of HAM's F12 (MediaTech, Herndon, VA) with 0.01% DNase I (Sigma) in a 60-mm Petri dish. The cell isolate was filtered through nylon mesh filters of 100 μm and 40 μm (BD Biosciences), successively, to remove aggregated cells and agarose. The cell suspension was centrifuged at 4°C. Cold lysis solution (5 ml) was added to the cell pellet for lysis of erythrocytes, and Dulbecco's modified Eagle medium (DMEM; Invitrogen) supplemented with 10% fetal bovine serum (FBS; Invitrogen) was added. The cell suspension was incubated with biotinylated anti-CD16/32 (anti-Fc receptor for macrophage) (BD Pharmingen, San Diego, CA) and anti-CD45 (for leukocyte) antibodies (BD Pharmingen) at 37°C for 30 minutes. After washing, the cell suspension was further incubated with streptavidin-coated magnetic particles (Promega, Madison, WI), and the cell suspensions were depleted of macrophages and leukocytes by magnetic cell separation (Promega). The remaining cells were incubated on 100-mm tissue culture dishes coated with mouse IgG (Jackson Immunoresearch Laboratories, West Grove, PA) for 2 hours at 37°C. The unattached cells were collected, and the suspension was centrifuged. The cell pellets were resuspended in DMEM supplemented with 10% FBS, and then plated on 100-mm culture dishes and placed in an incubator for 1 hour to allow for adhesion of lung fibroblasts. The unattached epithelial cells were collected for cytospin and RNA isolation. The attached cells were maintained and refed with DMEM supplemented with 10% FBS for lung mesenchymal cell culture. The cells were trypsinized and replated after about 5–7 days in culture. After passage one, the surviving cells in culture were composed almost entirely of fibroblasts.

Treatment of Mouse Lung Fibroblasts

Mouse lung fibroblasts were isolated as described previously here, and maintained in DMEM supplemented with 10% FBS, penicillin/streptomycin (Invitrogen), gentamicin (MP Biomedicals, Aurora, OH), and amphotericin B (Invitrogen). All treatments were performed with cells between two and four passages in 60-mm tissue culture dishes, unless otherwise noted. Cells isolated from wild-type and compound mutant mouse lungs were treated with FGF-1 (25 ng/ml), FGF-2 (25 ng/ml), heparin (5 μg/ml), or insulin-like growth factor (IGF)−1 (10–50 ng/ml). Treated and untreated cells were incubated at 37°C for 48 hours and then removed for RNA isolation.

Measurement of Stromal Cell–Derived Factor−1α and IGF-1

We measured the level of IGF-1 and stromal cell–derived factor (SDF)−1α/CXCL12 to validate the increased expression of these growth factors identified by microarray analysis. Whole lung tissue or freshly isolated AT2 cells were homogenized in RIPA buffer (Boston BioProducts, Worcester, MA) and protease inhibitor cocktail (catalog no. P8340; Sigma). The supernatant was collected for protein determination using the BCA colorimetric method (Thermo Fisher Scientific, Rockford, IL). Equal amounts of total protein from each sample were used for ELISA for IGF-1 and SDF-1α (R&D Systems, Minneapolis, MN) using the manufacturer's protocol. The results were represented as the total cytokine amount per total protein.

Statistical Analysis

Data are presented as means (±SEM). Statistical analysis for multiple comparisons was performed using one-way ANOVA with the Bonferroni correction. Student's unpaired *t* test was performed for analysis of two groups (MINITAB 14, State College, PA).

RESULTS

Failure to Thrive and Lung Hypoplasia in Mice Bearing Compound Mutations of FGFR3 and FGFR4

At birth, the appearance and body weight of FGFR3$^{-/-}$, FGFR4$^{-/-}$ compound mutant was indistinguishable from wild-type and littermate control animals, including FGFR3 mutant, FGFR4 mutant, FGFR3 heterozygote/FGFR4 mutant, and compound heterozygote mice (Figure 1A; see also Figure E1 in the online supplement). By Postnatal Day (P) 8, compound mutant mice displayed skeletal abnormalities, as previously described (19), and were clearly runted, with modestly reduced body weight. By P21, compound mutants were approximately 55% of the body weight of littermate control animals (Figure 1A). The emergence of these abnormalities was detected within the first week of age, whereas all pups displayed similar feeding patterns. No changes in the phenotype of compound mutants were observed when normal littermates were removed from the mother, further suggesting that the growth abnormalities were not a result of nutritional deficiency. FGFR3-deficient mice exhibited skeletal abnormalities identical to compound mutants (27), with intermediate total body weights (15.46 ± 1.65 g) not significantly different from either compound mutants ($P = 0.057$) or littermate control animals ($P = 0.482$) at P28. No gross abnormalities in lung size (or airspace structure) were observed in FGFR3-deficient mice, as previously noted.

Compound mutant mice developed outward symptoms of respiratory distress by approximately P21. Lung hypoplasia was noted, with an average lung weight at P28 of 50% of wild-type and compound heterozygote control animals (Figure 1B). Lung weight:body weight ratios in compound mutant mice were attenuated, but significantly less than in control animals (data not shown). Lung lobar structure was grossly normal in shape and arrangement (data not shown). These observations are consistent with those previously described for compound mutant mice in a mixed 129/Black Swiss background (19).

Quantitative Assessment of Airspace Enlargement in Mice Lacking FGFR3 and FGFR4

Alveogenesis initiates within 1 week of postnatal life in mice, and continues through the first month of postnatal life. We qualitatively (Figures 2A−2F) and quantitatively (Figures 2G and 2H) evaluated the ontogeny of airspace formation in wild-type, compound heterozygote, and compound mutant mice in the C57BL/6 background. At birth, the lungs of compound mutants were histologically indistinguishable from wild-type and compound heterozygote control animals, with all displaying pre–alveolar saccules of approximately similar size (Figures 2A and 2D). At P8, wild-type and compound heterozygote lungs displayed initiation of secondary crest formation and elongation (Figure 2B), whereas these structures were generally absent in compound mutant lungs (Figure 2E). By P28, wild-type and compound heterozygote lungs displayed a tremendous increase in structural complexity with formation of mature alveoli (Figure 2C). Compound mutant lungs continued to grow, but retained their simplified architecture, with rare secondary crest formation, resulting in gross airspace enlargement (Figure 2F). In addition to the abnormalities in airspace formation, compound mutant mice occasionally displayed mild mononuclear cell infiltration within the airspaces, squamous changes in the airway epithelium, and luminal airway exudates.

Using quantitative morphometric methods, we observed an anticipated decrease in airspace size (as defined by chord length or airspace area) between P8 and P28 in wild-type and compound heterozygote mouse lungs (Figures 2G−2H). Consistent with our histological observations demonstrating a failure in secondary crest formation/elongation, we observed a significant increase in airspace size in compound mutant lungs during the same time period. When compared with control animals, a modest increase in airspace size (as defined by chord length) was noted in compound mutant mice as early as P8. At P28, the compound mutants showed a 235% increase in mean chord length (Figure 2G), and a 480% increase in airspace area (Figure 2H), compared with control animals.

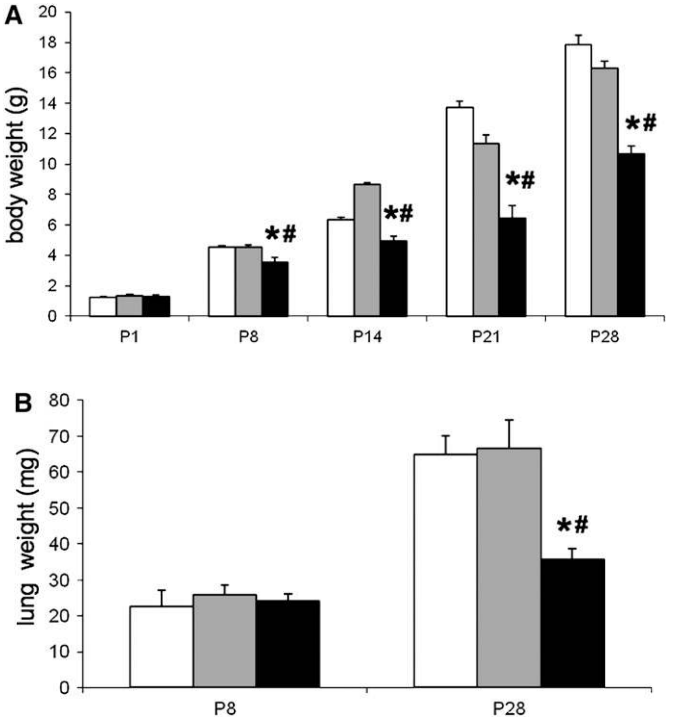

Figure 1. Growth characteristics of compound mutant mice. (*A*) Whole body weights of wild-type, FGFR3/4 compound heterozygous, and compound mutant mice during postnatal growth. Although no differences were noted between genotypes at birth, the weight of compound mutants was significantly less than age-matched control animals by 1 week of age (Postnatal Day [P] 8). (*B*) Lung weights of wild-type, FGFR3/4 compound heterozygous, and compound mutant mice during postnatal growth. Genotype-specific differences in lung weight were not observed before P8, whereas, at P28, lungs of compound mutants were approximately 50% of age-matched control animals. Data are presented as means (+SEM) (n = 9–12 mice in each group). *$P < 0.05$ with age-matched wild types. #$P < 0.05$ with age-matched compound heterozygotes. *Open columns* = wild type; *gray columns* = compound heterozygote; *solid columns* = compound mutant.

Genome-Wide Expression Profiles Indicate that Molecular Defects in Compound Mutant Mice Initiate after Birth

To characterize the molecular defects associated with the abnormality in lung maturation seen in compound mutant mice, we performed genome-wide expression profiling using Affymetrix Mouse Expression 430 2.0 microarrays. We profiled gene expression in triplicate for total lung RNA derived from wild-type, compound heterozygote, and compound mutant mice at P1, P8, and P28 (with the exception of P28, where only two arrays were completed for wild-type mice). These data are available at GEO (GSE15452). Unsupervised hierarchical clustering with bootstrap analysis (40) indicated that there were no global differences in molecular profiles at P1, but demonstrated

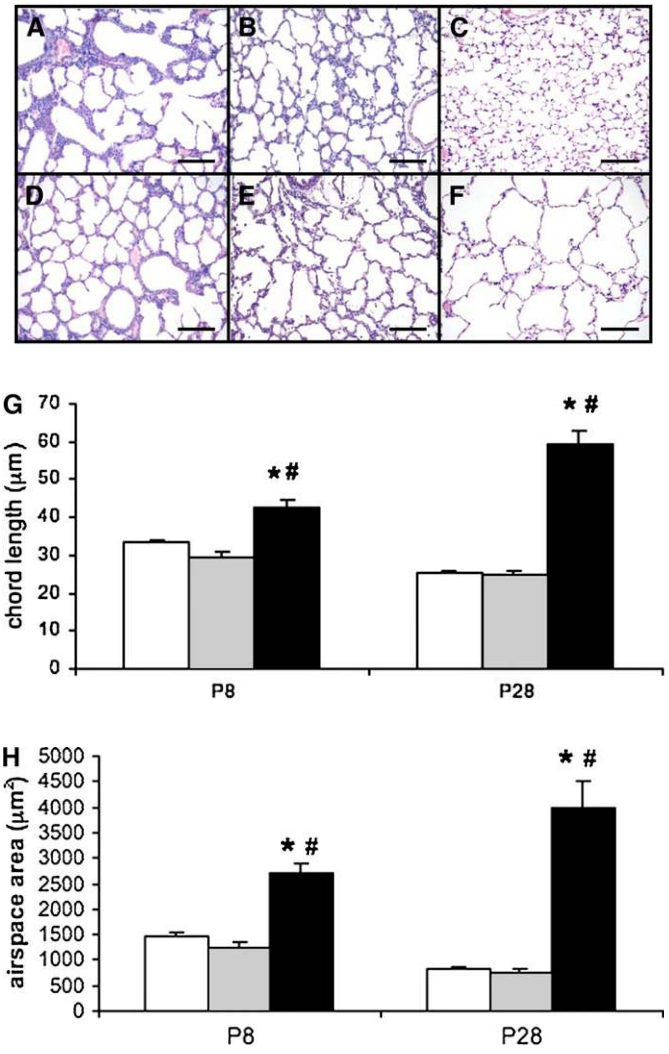

Figure 2. Qualitative and quantitative airspace ontogeny in compound mutant mice. (*A–F*) Shown are representative histology of lungs from control mice (*A–C*) and compound mutant mice (*D–F*) at Postnatal Day (P) 1 (*A* and *D*), P8 (*B* and *E*), and P28 (*C* and *F*). Note that all *panels* are presented at identical magnification. In control mouse lungs, the formation of secondary crests is evident at P8 (*B*), whereas minimal secondary crest formation is observed in age-matched compound mutant lungs (*E*). At P28, a tremendous increase in airspace complexity results from completed alveogenesis in control mice (*C*), whereas gross simplification resulting from expansion of primitive saccules is observed in compound mutant lungs (*F*). (*G* and *H*) Computer-assisted morphometry analysis quantified the mean linear distance between alveolar walls (chord length [*G*]) and mean size of individual airspaces (airspace area [*H*]) as detailed in METHODS. A significant decrease of chord length and airspace area in control mice between birth and P28 results from proper secondary crest initiation and elongation. Compound mutant mice at P8 and P28 display an increase in the size of airspaces over the same time period. Data are presented as means (+SEM) (n = 7–12 mice in each group). *$P < 0.05$ with age-matched wild types; #$P < 0.05$ with age-matched compound heterozygotes. (*A–F*) *Scale bars* = 100 μm; *open columns* = wild type; *gray columns* = compound heterozygote; *solid columns* = compound mutant.

a clear segregation of compound mutant profiles from controls at P8 and P28 (Figure 3). These data are consistent with histological and morphometric data, demonstrating that the defects in compound mutant lungs are not detectable at birth and initiate during the first week of postnatal life.

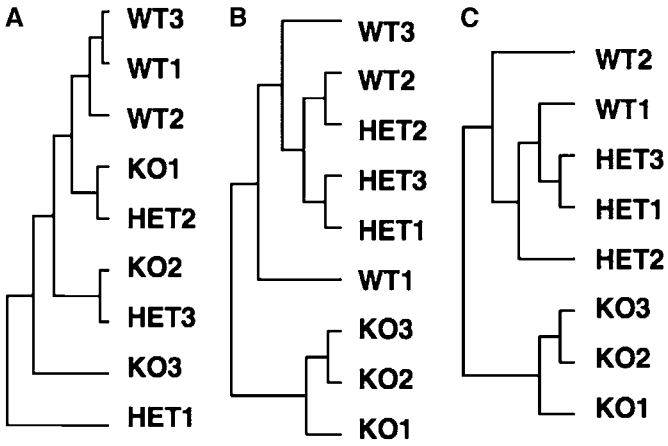

Figure 3. Molecular classification of lung genome-wide expression profiles. Global gene expression profiles were generated from pooled whole-lung RNA samples derived from wild-type (WT), compound heterozygous (HET), and compound mutant (knockout [KO]) mice. Shown are the global relationships between gene expression profiles among all samples, defined by unsupervised hierarchical clustering with Bootstrap analysis, at each time point. No segregation among genotypes was evident at P1 (*A*). At both P8 (*B*) and P28 (*C*), there was clear separation of compound mutant samples with both control groups, with 100% support (n = 3 arrays in each age–genotype group, except n = 2 arrays in WT at P28).

To identify genes dysregulated in compound mutant mouse lungs, which contribute to the distinction in global gene expression profiles, we performed statistical analysis of the microarray data. This analysis used a combination of SAM, GCOS Difference Calls, and t tests in an effort to improve reliability of gene identification and reduce false discovery (*see* METHODS). No genes consistently demonstrated evidence for differential expression in compound mutant lungs at P1 (data not shown), explaining the absence of segregation for the global profiles (Figure 3). At both P8 and P28, we identified groups of genes that were repeatedly defined as differentially expressed (*see* METHODS) according to SAM analysis of robust multichip average–derived data (at a median false discovery rate = 0) and consistent pair-wise GCOS Difference Calls. At P8, 23 probe sets, representing 20 genes, showed increased expression, and 17 probe sets, representing 15 genes, showed decreased expression in compound mutant lungs relative to both wild-type and compound heterozygote controls (Figure 4A). At P28, 74 probe sets, representing 57 genes, showed increased expression, and 68 probe, sets representing 46 genes, showed decreased expression in compound mutant lungs relative to both wild-type and compound heterozygote controls (Figure 4B and Table E1).

To appreciate consistent changes over the time course, we identified genes differentially expressed, as defined by the Difference Call algorithm alone, comparing compound mutants to compound heterozygotes at both P8 and P28. There were 13 genes showing increased expression, and 5 genes showing decreased expression in compound mutant mouse lungs at both P8 and P28 compared with age-matched compound heterozygotes. Genes with consistently increased expression included those related to: ECM (asporin [Aspn], microfibrillar-associated protein 5 [Mfap5], tropoelastin [Eln]); receptor and signal transduction (endothelin 1 [Edn1], Igf1, neurotrophic tyrosine kinase receptor, type 2 [Ntrk2], SDF-1/CXCL12 [Sdf-1/Cxcl12]); enzyme and inhibitor (S-adenosyl methionine decarboxylase [Amd1], serine peptidase inhibitor, Kazal type 5 [Spink5]); transport (lipocalin 2 [Lcn2], sodium-taurine cotrans-

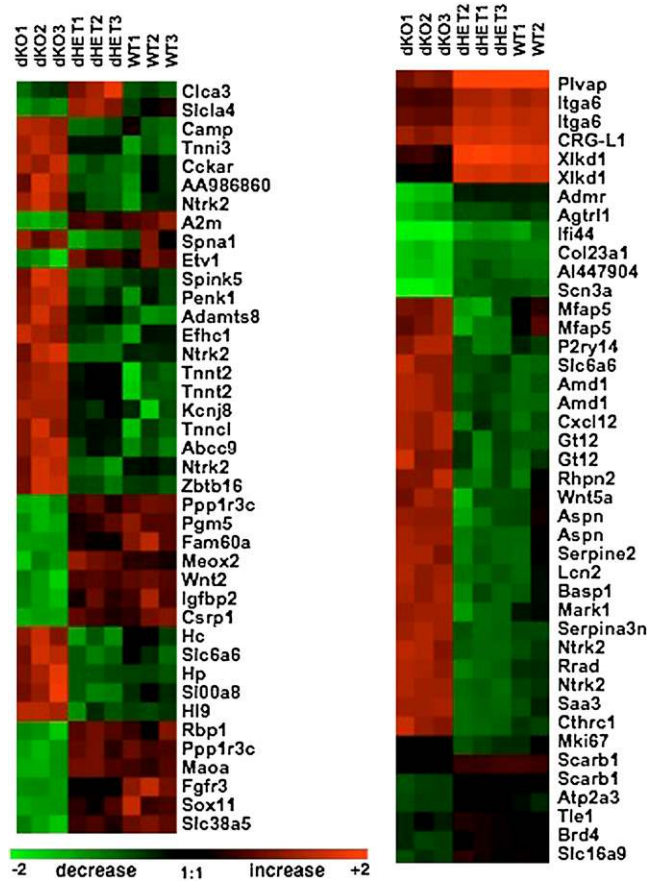

Figure 4. Gene discovery in compound mutant lungs. Global gene expression profiles were generated from pooled whole-lung RNA samples derived from wild-type (WT), compound or double heterozygous (dHET) and compound or double mutant (dKO) mice. Differential expression for individual genes was defined separately, at P8 (*left*) or P28 (*right*), using a combination of statistical criteria, as described in METHODS. Normalized signal intensity measurements are shown for each of the genes identified as significantly differentially expressed (*rows*) among individual samples (*columns*), with *red* indicating a relatively high level of expression, and *green* representing a relatively low level of expression. Due to space constraints, a limited subset of genes with the greatest evidence for differential expression at P28 is presented; the complete list of genes is provided in Table E1.

porter [Slc6a6], mesothelin [Msln], metallothionein 1 [Mt1]). Genes with consistently reduced expression included those related to receptor and signal transduction (hyaluronan receptor [Xlkd1], FGFR3 [Fgfr3], IGF binding protein 2 [Igfbp2], integrin-α6 [Itga6]) and transcriptional regulation (SRY-box containing gene 11 [SOX11]). Some significantly dysregulated genes (Aspn, Mfap5, Ntrk2, Amd1, and Xlkd1) were represented by more than one probe set.

Coordinated Elastic Fiber Gene Dysregulation in Compound Mutant Mice

Among the genes identified as dysregulated in compound mutant mice were two elastic fiber proteins, Eln and MFAP5/microfibril-associated glycoprotein 2. We sought to test for a broad induction of genes essential for elastic fiber formation including fibrillin 1, fibulin 1, fibulin 5, lysyl oxidase (LOX), LOX-like 1 (LOXL1) using qPCR. We confirmed a significant ($P < 0.05$) induction of Eln (11-fold) and MFAP5 (twofold) in compound mutant mice as compared with control animals, and identified coordinated significant increases in the expression of fibrillin 1 (threefold), fibulin 1 (threefold), fibulin 5 (fivefold), lysyl oxidase (fourfold), and lysyl oxidase-like (fivefold) at P28 (Figure 5). It is important to note that the absolute expression levels of elastic fiber proteins decreases between P8 and P28 in wild-type mice.

To confirm that changes in mRNA levels coincided with elastic fiber deposition, we biochemically measured lung elastin content by desmosine radioimmunoassay (Figure 6A and Figure E3). Lung elastin content, as a ratio of total protein (desmosine:total protein), was increased in compound mutant mice versus age-matched control animals (both wild type and compound heterozygote) as early as P8, and persisted through P28. Total protein content in compound mutant lungs was not significantly affected at P8, but was significantly decreased at P28 compared with the controls. Total elastin content was not found to be different among genotypes within each age group (Figure 6A). The small but significant difference in elastin content noted at P8 (at the onset of elastic fiber gene expression) precedes significant changes in elastic fiber gene expression in compound mutant lungs, and likely reflects changes in lung structure (changes in ratio of vascular/airway versus airspace elastin). However, a modest increase in a number of elastic fiber genes was noted as early as P8, which may have led to cumulative increases in elastic fiber content.

In the maturing alveolus, elastic fibers are primarily deposited at the tips of elongating secondary crests, which will form alveolar entrance rings. We used a modified Hart's stain to examine the spatial distribution of elastic fibers in the lung (Figures 6B–6E). Histochemical staining demonstrated that newborns of all genotypes had elastic fibers of normal appearance in large muscularized vessels, in the media of conducting airway walls, and, to a lesser extent, within the airspaces (data not shown). Comparable elastic fiber deposition was observed in the conducting airways and vasculature of mutant and control mice at all time points studied. In control mice, between P8 and P28, airspace elastic fibers became prominent and were spatially restricted, with accumulation at the tips of elongating secondary crests (Figures 6B and 6C). Compound mutant mice failed to form/elongate secondary crests, but exhibited a marked increase in elastic fiber staining (Figures 6D and 6E) throughout the airspace wall. No spatial restriction in elastic fiber accumulation, as observed in normal control lungs, was apparent.

Absence of Lung Fibroblast Elastogenesis Defects in Compound Mutant Mice

Exogenous FGFs can suppress mesenchymal cell elastin gene expression (41, 42). Therefore, excessive elastogenesis in the lungs of FGFR3/4-deficient mice could be due to the loss of FGF-mediated repression of lung fibroblast elastic fiber gene expression. To determine the mechanisms mediating aberrant elastic fiber production, we evaluated gene expression in lung fibroblasts from wild-type and compound mutant mice *in vitro*. Primary lung fibroblasts were isolated from 3- to 4-week-old lungs and grown to confluence and assayed at low passage. We examined expression of fibroblast FGFR3 and FGFR4 by qPCR in wild-type cells, and found low to moderate levels of expression (data not shown). The baseline expression levels of most elastic fiber genes in these cells were not significantly different between compound mutant and wild-type fibroblasts (Figure 7). We did note a modest but significant decrease in the baseline expression of fibrilin 1 in the compound mutant fibroblasts. A number of additional genes identified as dysregulated in the microarray data were assayed in fibroblast cultures and found to be similar between compound mutant and controls (data not shown). These data indicate that, although there are

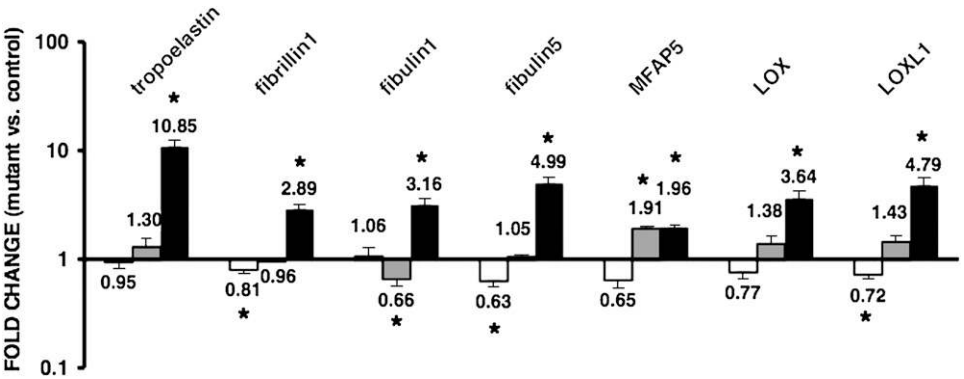

Figure 5. Coordinated induction of elastic fiber genes in compound mutant lungs. Expression of genes related to elastic fiber formation, assembly, and cross-linking were assessed by quantitative real-time PCR in whole-lung RNA from wild-type, compound heterozygous, and compound mutant mice. The numbers at each *bar* indicate the magnitude of fold change in compound mutant lungs relative to that in age-matched compound heterozygote lungs. Significant increases in expression for all genes were noted at Postnatal Day (P) 28, coincident with airspace enlargement. Data are presented as means (±SEM) (n = 7–12 mice in each group). *$P < 0.05$ with age-matched control animals. LOX = lysyl oxidase; LOXL = LOX-like; MFAP = microfibrillar-associated protein. *Open columns* = P1; *gray columns* = P8; *solid columns* = P28.

effects resulting from deficiency in FGFR3 and FGFR4, they do not account for increased elastic fiber gene expression and deposition *in vivo*. To further explore the phenotype of compound mutant fibroblasts, we investigated the repressive effects of FGF ligands on elastin gene expression. Fibroblasts were treated with FGF1 or FGF2, ligands for FGFR1–4, in the absence or presence of exogenous heparin, a cofactor for FGFR activation. We confirmed that FGF1 and FGF2 broadly suppress expression of elastic fiber protein genes in primary lung fibroblast cultures derived from control mice (Figure 7). Similar repressive effects of FGF ligands, or heparin alone, were observed in fibroblast cultures derived from compound mutant mice. These data indicate that the repressive effects of FGF upon elastic fiber gene expression are mediated by FGFR1 and/or FGFR2, and are consistent with the conclusion that the elastogenesis defects in compound mutant mice are not fibroblast cell autonomous.

Alterations in Alveolar Epithelial Cell Phenotype in Compound Mutant Mice

It is known that the lung epithelium can influence adjacent mesenchymal cell phenotype (43, 44). Therefore, we considered type II epithelial cells as a source for primary defects leading to aberrant mesenchymal cell elastogenesis in compound mutant mice. Microarray analysis of the molecular phenotype in compound mutant mice suggested dysregulation of a number of potential paracrine factors, including Igf1, Igfbp2, Wnt5a, and Sdf1α/Cxcl12. qPCR of whole-lung RNA confirmed significant increases in the expression of Igf1 and Wnt5a in compound mutant lungs—specifically at P8, the time of onset for pathogenesis (Figure 8A). We also confirmed a coordinated decrease in expression of the Igf1 binding protein, Igfbp2, an additional mechanism that could contribute to excessive bioavailability of this pro-elastogenic factor.

We isolated AT2 from 3- to 4-week-old compound mutant and wild-type mice using standard methods, and tested freshly isolated cells as the source for abnormal expression of the paracrine factors. Purity of the AT2 cell preparations was comparable between genotypes, as defined by SP-C immunocytochemistry (ranged from 85 to 95% positive cells) and by the expression level of SP-C mRNA, which was not different between groups, as defined by qPCR (data not shown). We confirmed expression of FGFR3 and FGFR4 in control AT2 by qPCR, indicating that they are candidates for primary defects in compound mutant mice (data not shown). We identified significant increases for Igf1 and Sdf1α expression in AT2 from compound mutant mice as compared with control animals (Figure 8B). Significant differences were evident when expression was normalized to the housekeeping gene, cyclophillin A, or the marker of AT2 cells (purity), Sftpc. Modest but nonsignificant changes were observed in the expression of Igfbp2 and Wnt5a (data not shown). Finally, we tested whether increased expression at the mRNA level was associated with increases in the bioavailability of these molecules. We found a significant increase in SDF1α protein levels in whole-lung homogenates derived from compound FGFR3/4 mutant mice (Figure 8C). Together, these data identify primary defects in compound mutant AT2 cells, and show that they express abnormal levels of paracrine factors, including increases in the proelastogenic cytokine, Igf1.

Increased Number of Elastogenic Cells in Compound Mutant Mice

Distal lung fibroblast heterogeneity during development has been appreciated, with airspace elastic fibers produced during alveogenesis by a subpopulation of αSMA-expressing mesenchymal cells. Excessive and disorganized elastic fiber deposition in compound mutant mice could be due to either an increase in production of elastic fiber proteins from a normal number of elastogenic fibroblasts or the presence/recruitment of an increased number of elastogenic cells. As indicated previously here, there was no induction in baseline elastic fiber gene expression observed in isolated lung fibroblasts from compound mutant lungs. Conversely, immunohistochemistry revealed increased αSMA expression in the distal lungs of compound mutant mice at P8 (Figure 9), coincident with the initiation of excessive elastogenesis.

To determine whether cell proliferation contributes to excessive elastogenesis and enhanced αSMA expression in compound mutant mice, we examined airspace cell proliferation (Figures 10A−10B). Similar to other molecular and histological features, we observed no changes in the proliferative index (defined as the percentage of Ki67 positive–staining cells) between genotypes at P1 (Figure 10C). However, the proliferative index was significantly reduced in compound mutant mice throughout alveogenesis (between P8 and P28). Interestingly, the total number of cells (defined as the total number of nuclei per field) in the alveolar wall during this period was not significantly different among genotypes, suggestive of a higher cell density in compound mutant airspace walls. These data suggest an increase in the proportion of elastogenic cells in compound mutant lungs that is not due to increased proliferation of these cells *in situ*.

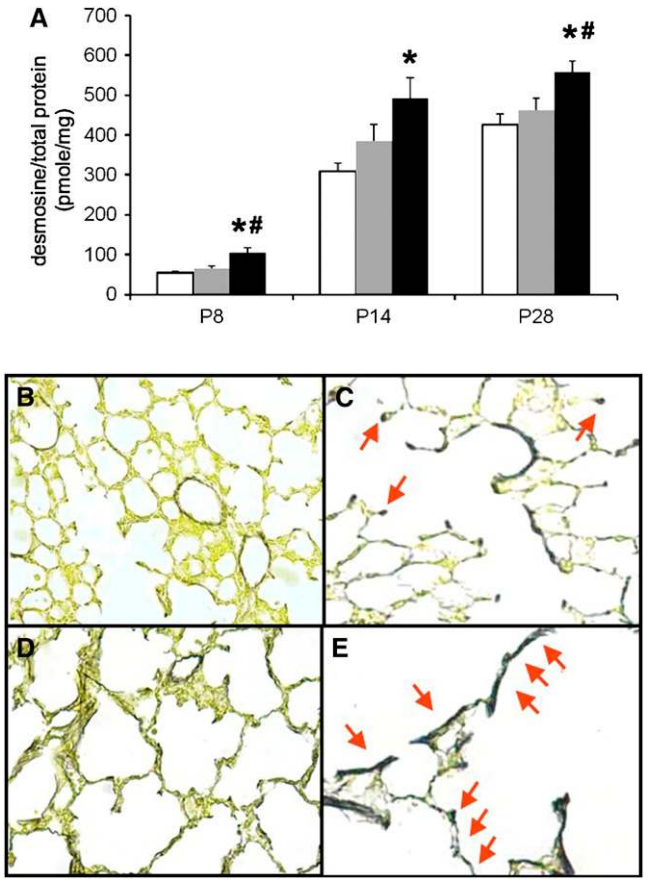

Figure 6. Excessive and disorganized elastic fiber accumulation in compound mutant mice. (*A*) Elastin content, defined as the ratio of desmosine/isodesmosine to total protein, was determined in whole lung tissue derived from wild-type, compound heterozygous, and compound mutant mice. A significant increase in elastin content was observed in compound mutant lungs at all time points studied, as early as Postnatal Day (P) 8. Data are presented as means (+SEM) (n = 7–12 mice in each group). *$P < 0.05$ with age-matched wild types; #$P < 0.05$ with age-matched compound heterozygotes. *Open columns* = wild type; *gray columns* = compound heterozygote; *solid columns* = compound mutant. (*B–E*) Shown are representative images of control (*B* and *C*) and compound mutant (*D* and *E*) lungs stained for elastic fibers using a modified Hart's procedure. Elastic fibers are stained *black* with *yellow* counterstain. Elastic fibers are rich in vascular and airway structures prior to birth. In control mice, airspace elastic fibers accumulate at the tips of elongating secondary crests beginning before 1 week of age, and are restricted to this location in mature alveoli (*red arrows* in *B* and *C*). Excessive elastic fiber accumulation is apparent by P8 in compound mutant lungs, and appears throughout the wall of enlarged airspaces in the absence of secondary crests at P28 (*red arrows* in *D* and *E*). Relative magnification = 100× (*B* and *D*); 400× (*C* and *E*).

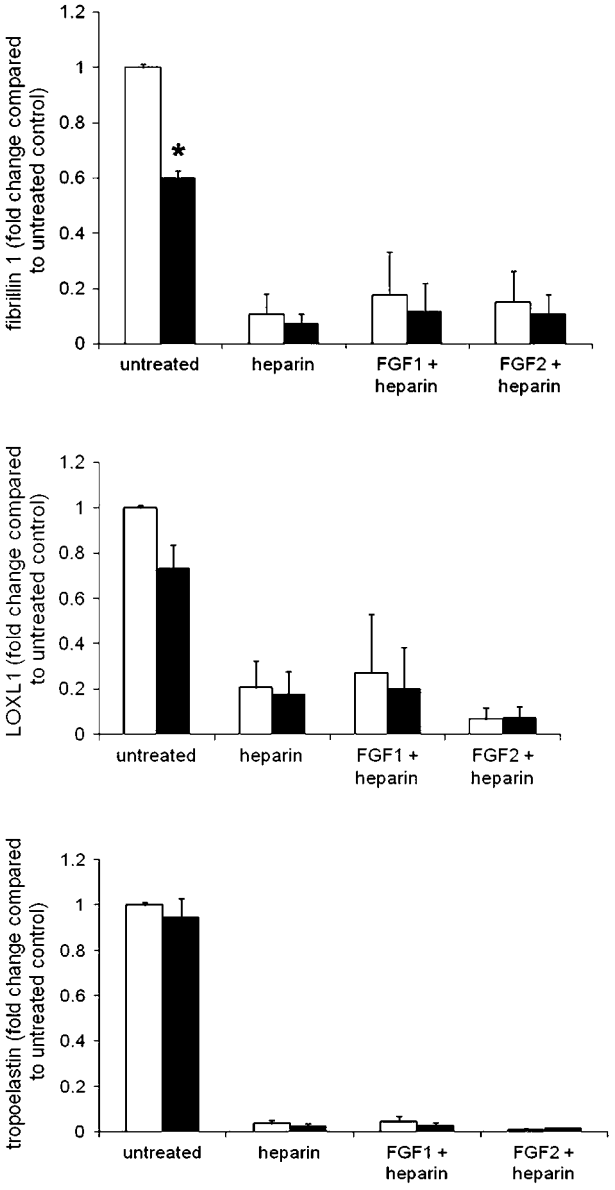

Figure 7. Normal elastic fiber gene expression in isolated mouse lung fibroblasts. Elastic fiber gene expression was assessed in primary cultures of mouse lung fibroblasts isolated from wild-type and compound mutant mice. Steady-state gene expression was determined for confluent cultures grown under standard conditions (untreated) or after stimulation with the nonspecific fibroblast growth factor (FGF) receptor ligands, FGF1 and FGF2, in the presence of heparin, or with heparin alone as a control. No increases in the expression of Eln, fibrillin 1 or lysyl oxidase-like 1 were observed in untreated compound mutant cells. Furthermore, compound mutant fibroblasts demonstrated normal repression of elastic fiber gene expression upon treatment with exogenous FGFs, or activation of endogenous FGFs with heparin. Data represent the fold change in treated fibroblast relative to wild-type nontreated fibroblast controls. Data are means (+SEM) (n = 3 experiments in each group). *$P < 0.05$ with treatment-matched wild-type cells. *Open columns* = control; *solid columns* = compound mutant.

IGF1 Stimulates Lung Fibroblast Elastin Expression

IGF1 has been appreciated as a stimulator of elastin expression in nonpulmonary elastic cells/tissues (45–48). Interestingly, lung expression of IGF1 and IGF1 receptor (IGF1R) has been demonstrated (49), and deficiency in either IGF1, or its cognate receptor, IGF1R, results in neonatal lethality and lung development abnormalities (50, 51). However, details regarding the histopathology of these mice are lacking. Conflicting data exist regarding the ability of IGF1 to promote lung fibroblast elastin expression (52, 53). We attempted to reassess the regulatory effects of IGF1 on lung fibroblast elastin expression. We found that short-term (24–48 h) treatment of primary confluent cultures of mid-passage (p2–4) mouse lung fibroblasts with IGF1 (10–50 ng/ml) resulted in no changes in elastin gene expression (data not shown). Conversely, as shown in Figure 11, when subconfluent cultures of newly explanted lung fibroblasts were exposed to long-term treated with IGF1 (50 ng/ml for

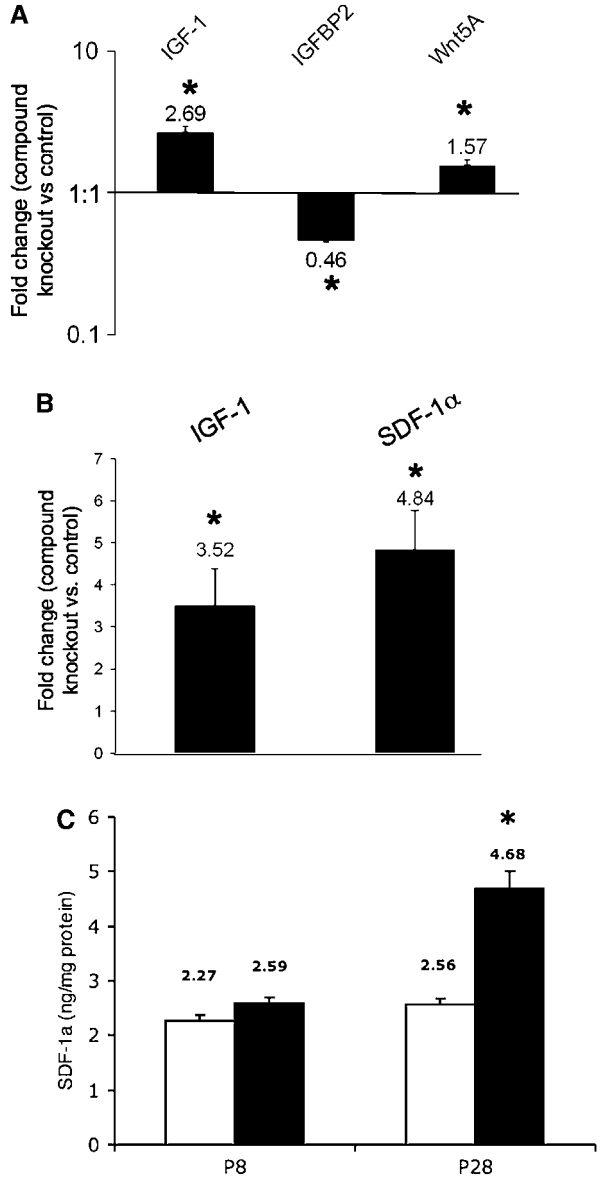

Figure 8. Abnormal alveolar epithelial cell growth factor expression in compound mutant mice. (*A*) Expression of growth factors identified as dysregulated in microarray data (insulin-like growth factor [IGF] 1, Igf binding protein [IGFBP] 2, Wnt5a) were assessed by quantitative real-time PCR (qPCR) in whole mouse lung RNA from wild-type and compound mutant mice at Postnatal Day (P) 8. The numbers at each *bar* indicated the magnitude of fold change in compound mutant lungs relative to that in age-matched control lungs. Data are presented as means (±SEM) (n = 7–12 mice in each group). *$P < 0.05$ with age-matched controls. (*B*) Expression of epithelial cell paracrine factors, IGF1, and stromal cell–derived factor (SDF) 1α, was assessed by qPCR in freshly isolated type II pneumocyte cell RNA from wild-type and compound mutant mice. Data are presented as means (+SEM) (n = 5–7 cell isolates in each group). *$P < 0.05$ with age-matched controls. (*C*) Expression of SDF1α was assessed by ELISA in whole-lung lysates from wild-type and compound mutant mice at P8 and P28. *Open columns* = control; *solid columns* = compound mutant. Data are presented as means (+SEM) (n = 8–10 lungs in each group). *$P < 0.05$ with age-matched wild type.

14 d), we observed a consistent and robust induction of elastin gene expression (7.5-fold; $n = 3$; $P < 0.05$). The magnitude of this response was greater than that observed for other physiological inducers of elastin gene expression, such as TGFb or retinoic acid (54, 55).

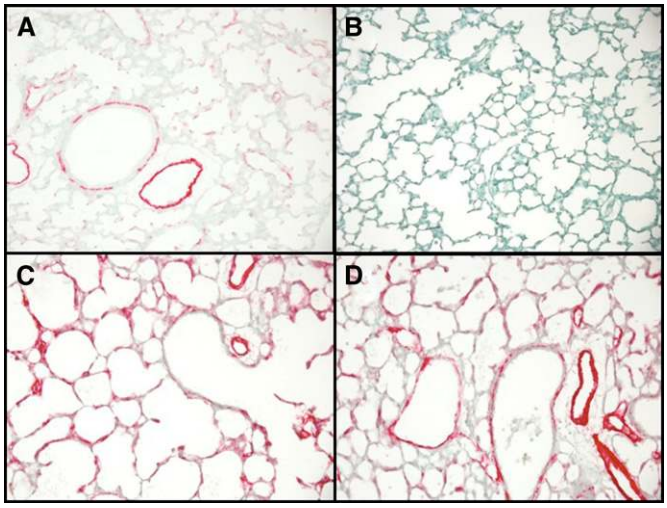

Figure 9. Increased airspace α-smooth muscle actin (αSMA) expression in compound mutant mice. The amount of elastogenic αSMA-expressing cells in Postnatal Day (P) 8 airspaces of wild-type (*A*) and compound mutant (*C* and *D*) lungs was assessed by immunohistochemistry. Immunoreactivity is observed as *red staining* with a *green counterstain*. Nonspecific IgG (*B*) was used as a staining control. Although similar staining patterns are observed between genotypes in vascular and airway structures, an increase in αSMA staining in the alveolar walls of compound mutant mice is apparent.

DISCUSSION

FGF signaling is critical throughout all stages of lung development (56, 57). FGFR3 and FGFR4 signaling, in particular, appears to be critical for alveogenesis. We have confirmed that mice with combined deficiency of FGFR3 and FGFR4 develop postnatal airspace enlargement, here in a pure C57BL/6 background. We show that histological, morphometrical, biochemical, and molecular data are consistent with lung abnormalities initiating after birth in these mice. This conclusion is supported by quantitative assessment of lung structure and genome-wide expression profiling. We have also confirmed abnormalities in airspace elastic fiber production in compound mutant mice, and demonstrated that this involves coordinated overproduction of all elastic fiber components and accumulation of excessive elastic fibers lacking typical spatial restriction at alveolar entrance rings. We show that these abnormalities are not due to fibroblast-autonomous defects, but are associated with excessive production of AT2 paracrine factors capable of increasing alveolar fibroblast elastin expression. Finally, we demonstrate that the excessive, misplaced elastic fiber accumulation is associated with an apparent increase in the number of elastogenic alveolar mesenchymal cells expressing αSMA. Our data are consistent with the conclusion that defective AT2 paracrine signaling contributes to abnormal elastogenesis.

Compound FGFR3/4 mutant mice exhibit dwarfism and lung hypoplasia. Whether the dwarfism phenotype can exclusively account for the decrease in lung size is unknown. Interestingly, Klotho mutant mice (58), Fgf23 mutant mice (59), and Hoxa5 mutant mice (60) were reported to exhibit growth retardation associated with the decreased lung size and postnatal airspace enlargement. However, FGFR3 mutant mice develop impaired growth, but no failure of alveolar septation (e.g., airspace enlargement) was reported (27) nor observed in our studies.

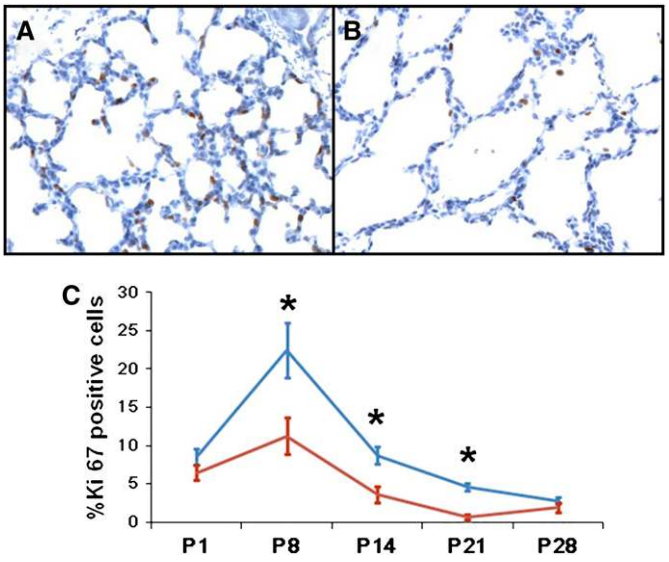

Figure 10. Decreased airspace cell proliferation in compound mutant mice. Immunohistochemistry for Ki67 was used to assess cell proliferation in airspaces of wild-type (*A*) and compound mutant (*B*) lungs at Postnatal Day (P) 8. Immunoreactivity is observed as *brown staining* for Ki67 with *blue counterstained* nuclei. Nonspecific IgG was used as a staining control (data not shown). A proliferative index (*C*) was determined by counting the percentage of Ki67-positive cells (number of Ki67-positive–staining cells relative to the total nuclei per high-power field) in the airspace walls of wild-type(*top line*) and compound mutant (*bottom line*) lungs. Although similar proliferation rates are noted between genotypes at birth, a significant reduction in proliferation is noted in P8, P14, and P21 in compound mutant mice. Data are presented as means (±SEM) (n = 7–12 mice in each group). *$P <$ 0.05 with age-matched controls.

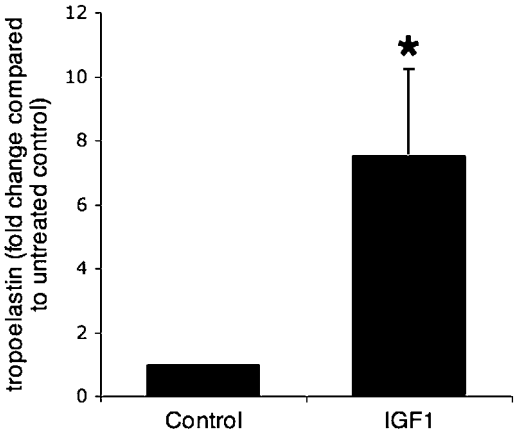

Figure 11. Increased elastin expression in insulin-like growth factor (IGF) 1–treated lung fibroblasts. Elastic fiber gene expression was assessed in primary cultures of mouse lung fibroblasts isolated from wild-type mice. Steady-state gene expression was determined for subconfluent explant cultures grown under standard conditions (Control) or after stimulation with IGF1 (50 ng/ml) for 14 days. Data represent the expression level in IGF1-treated relative to nontreated control animals. Data are means (+SEM) (n = 3 experiments). *$P <$ 0.05.

Therefore, we conclude that the dwarfism phenotype in compound mutant mice is not sufficient to explain alveogenesis defects. However, the data clearly suggest cooperative roles of FGFR4 with FGFR3 in coordinating body growth and lung development.

The role of FGFR signaling in airspace formation was also studied using transgenic mice expressing a soluble dominant-negative FGFR in the lung (61–62). Embryonic inhibition of FGF resulted in abnormal airspace enlargement, whereas postnatal inhibition had no effect on alveogenesis, suggesting that FGFR function was critical during the prenatal period. These data are inconsistent with our current studies, which failed to identify any deficiencies at birth in compound mutant mice. Potential technical differences, including receptor specificity and expression patterns for the dominant-negative FGFR transgene, could explain the differences in these models. It is possible that the genomic, histological, biochemical, and molecular approaches that we used in the current study were not sensitive enough to identify specific prenatal changes that may exist in compound mutant mice. However, it is likely that failed alveogenesis in compound mutant mice results predominantly from postnatal effects.

Previous studies have described temporal and cell type–specific expression of FGFR3 and FGFR4 during lung development (19–21, 63). We sought to define the FGFR3/FGFR4–dependent mechanisms of alveolar formation during postnatal lung development in compound mutant mice using microarray analysis coincident with the histopathological observations. The genomic profiles revealed, among a small number of genes, the induction of multiple genes related to elastic fiber assembly in compound mutant mice. We validated these changes and observed coordinated induction in additional genes related to elastic fiber assembly, including tropoelastin, microfibril-related proteins (fibrillin-1, Mfap5 or microfibril-associated glycoprotein 2, fibulin 1, fibulin 5), and lysyl oxidases, Lox and Loxl1, all of which are essential for elastogenesis. Histochemical and biochemical analyses corroborated the findings at the mRNA level, confirming increased elastic fiber deposition in compound mutant lungs.

Decreased elastic fiber formation has been associated with airspace abnormalities in numerous gene-targeted animal models: elastin (12); RAR/RXR (15); fibrillin-1 (13); loxl1 (64); fibulin (65). Excessive, disorganized elastic fiber accumulation can be a histopathological feature of impaired airspace formation in human bronchopulmonary dysplasia (66) and in several animal models of this disease (17, 67–70). Reduced expression of FGFR3 and FGFR4 was observed in rodent models of BPD induced by neonatal hyperoxic exposure (17, 18, 71), suggesting that impaired alveogenesis and excessive elastic fiber accumulation observed in these models may partly result from alterations in FGFR signaling. In total, these data indicate that appropriate quantitative and spatial deposition of elastic fibers is critical for normal airspace formation and lung function. We have not defined whether excessive elastogenesis observed in this model is causative for the failure of secondary crest elongation. Deficiencies in septation likely affect lung mechanics. Therefore, the overproduction of elastic fibers could be a compensatory response. Interestingly, our data are consistent with the conclusion that increased elastin accumulation in this model is a result of persistence of elastin gene expression in the compound mutant mouse at P28 when expression is repressed in the wild-type lung.

It is important to note that elastogenesis in the lung vasculature and airways, and in other tissues, was normal in compound mutant mice. This reinforces the specificity of the defect, and indicates that distinct regulatory mechanisms contribute to airspace elastic fiber production. We investigated lung fibroblasts to determine the mechanism for aberrant airspace elastogenesis in compound mutant mice. No induction in baseline or regulated

elastic fiber gene expression, or any other abnormalities, were observed in mutant fibroblasts. No change in the expression of TGF-β1, which is thought to function as an autocrine inducer of lung fibroblast elastin production (72), was found in the microarray data or by qPCR. Additional experiments were performed to identify differences in isolated fibroblasts derived from both wild-type and mutant mice. Heparin treatment, likely through activation of endogenous FGF activity, or exogenous FGF treatment resulted in similar inhibitory responses in both wild-type and mutant fibroblasts. Our data suggest that dysregulation of elastic fiber genes *in vivo* is not a primary defect in lung fibroblasts, and that another cell type provided paracrine signals involved in the regulation of elastogenesis.

Conversely, we found changes in the expression of multiple paracrine factors from AT2 cells, including the elastogenic molecule, Igf1 (53, 73, 74), and its binding protein, Igfbp2. Interestingly, lung expression of IGF1/IGF1R has been demonstrated (49), and deficiency in either IGF1 or IGF1R leads to abnormal lung development (50, 64). The cellular and molecular mechanisms contributing to this phenotype have not been defined. Conflicting data exist regarding the ability of IGF1 to promote lung fibroblast elastin expression. One prominent study reported tissue specificity for the inductive effects of IGF1 on elastin expression, with a lack of response in lung fibroblasts (52). However, an earlier study suggested some potential elastogenic effects of IGF1 in lung fibroblasts (53). We observed an inductive response that was greater than that observed for other physiological inducers of lung fibroblast elastin gene expression, such as TGFβ or retinoic acid (54, 64). These data implicate epithelial–mesenchymal interactions in the regulation of airspace elastogenesis and its dysregulaiton in compound mutant mice. Additional factors, including peptides (e.g., TGFβ), hormones (retinoic acid), and physical forces are also likely to contribute to the regulation of airspace elastin gene expression during development.

Airspace mesenchymal cell heterogeneity, including, but not limited to, myofibroblasts, lipid-laden fibroblasts, and pericytes, has been well documented. Physiologically, airspace elastin is primarily produced by αSMA-expressing fibroblasts located at alveolar septal tips (75), resulting in elastic fiber enrichment at alveolar entrance rings. Recent reports have demonstrated that appropriate FGF signaling is essential for myofibroblast differentiation and induction of αSMA expression during alveogenesis (62). In compound FGFR3/FGFR4 mutant mice, we demonstrate a spatially unrestricted deposition of elastic fibers throughout the primary saccular wall. This was accompanied by an increase in αSMA immunostaining. The increase in elastogenesis and αSMA expression was coincident with a significant reduction in airspace cell proliferation, suggesting either excessive recruitment of elastogenic cells or a failure of differentiation and/or proliferation of nonelastogenic fibroblasts, normally found at the base of secondary crests. Interestingly, compound mutant AT2 cells showed increased expression of SDF1α. This molecule is a regulator of progenitor cell recruitment, vascular cell differentiation, and angiogenesis (76–78), and has previously been shown to be suppressed by FGF signaling (79, 80).

Our current studies have a number of limitations. We used standard morphometry of liquid-inflated, constant pressure–fixed lungs. The objectives of this analysis were to quantify the magnitude of changes in airspace size, and to track the relative sizes of the airspaces of compound mutant mice during maturation. We acknowledge that the structural and biochemical changes may have significant effects upon pressure-normalized inflation, and that alternate methods of morphometric analysis would likely result in quantitative differences. However, given the magnitude of the abnormal pathology, the relative differences and our conclusions are unlikely to be changed. Another limitation concerns our studies of isolated fibroblasts. How the phenotype of these cultured cells resembles the population responsible for elastin expression *in vivo* is not clear. For instance, it unavoidably removes factors such as mechanical loading. Although our data indicate that excessive elastic fiber production from these cells reflects a response to paracrine factors, it would be premature to conclude that compound mutant fibroblasts are not actively involved in the lung pathology observed in these mice.

In conclusion, we have demonstrated that FGFR3/FGFR4 signaling contributes to the spatiotemporal specification of lung elastic fiber production. Mice with compound mutation of FGFR3/FGFR4 display disrupted postnatal lung growth, with airspace enlargement and excessive elastic fiber deposition. *In vitro* studies demonstrate that induction of elastin expression is not a primary defect in fibroblast cells *per se*, but result from paracrine signaling from airspace epithelial cells. Current studies focus on defining the mechanisms of Igf1 and Sdf1α upon lung mesenchymal cell differentiation and specification, which may represent a novel, airspace-specific mechanism regulating elastogenesis.

Conflict of Interest Statement: S.S. received lecture fees from Pharmalink up to $1,000. S.B. does not have a financial relationship with a commercial entity that has an interest in the subject of this manuscript. D.M.S. does not have a financial relationship with a commercial entity that has an interest in the subject of this manuscript. S.K.S. does not have a financial relationship with a commercial entity that has an interest in the subject of this manuscript. S.T. does not have a financial relationship with a commercial entity that has an interest in the subject of this manuscript. B.S. received grant support from Vatrix ($10,001–$50,000). T.J.M. does not have a financial relationship with a commercial entity that has an interest in the subject of this manuscript.

Acknowledgment: The authors recognize the contributions of Dr. Meltem Arikan, Temana Andalcio, Roberto Landazury, Jungha Hong, and Alyssa McCoy in support of the studies described in this article.

References

1. Davies G, Reid L. Growth of the alveoli and pulmonary arteries in childhood. *Thorax* 1970;25:669–681.
2. Hyde DM, Blozis SA, Avdalovic MV, Putney LF, Dettorre R, Quesenberry NJ, Singh P, Tyler NK. Alveoli increase in number but not size from birth to adulthood in rhesus monkeys. *Am J Physiol Lung Cell Mol Physiol* 2007;293:L570–L579.
3. Thurlbeck WM. Postnatal growth and development of the lung. *Am Rev Respir Dis* 1975;111:803–844.
4. Thurlbeck WM. Lung growth and alveolar multiplication. *Pathobiol Annu* 1975;5:1–34.
5. Tuder RM, McGrath S, Neptune E. The pathobiological mechanisms of emphysema models: what do they have in common? *Pulm Pharmacol Ther* 2003;16:67–78.
6. Zhang MC, He L, Giro M, Yong SL, Tiller GE, Davidson JM. Cutis laxa arising from frameshift mutations in exon 30 of the elastin gene (ELN). *J Biol Chem* 1999;274:981–986.
7. Loeys B, Nuytinck L, Van Acker P, Walraedt S, Bonduelle M, Sermon K, Hamel B, Sanchez A, Messiaen L, De Paepe A. Strategies for prenatal and preimplantation genetic diagnosis in Marfan syndrome (MFS). *Prenat Diagn* 2002;22:22–28.
8. Shinawi M, Boileau C, Brik R, Mandel H, Bentur L. Splicing mutation in the fibrillin-1 gene associated with neonatal Marfan syndrome and severe pulmonary emphysema with tracheobronchomalacia. *Pediatr Pulmonol* 2005;39:374–378.
9. Cupo LN, Pyeritz RE, Olson JL, McPhee SJ, Hutchins GM, McKusick VA. Ehlers-Danlos syndrome with abnormal collagen fibrils, sinus of Valsalva aneurysms, myocardial infarction, panacinar emphysema and cerebral heterotopias. *Am J Med* 1981;71:1051–1058.
10. Warburton D, Gauldie J, Bellusci S, Shi W. Lung development and susceptibility to chronic obstructive pulmonary disease. *Proc Am Thorac Soc* 2006;3:668–672.
11. Wagenseil JE, Mecham RP. New insights into elastic fiber assembly. *Birth Defects Res C Embryo Today* 2007;81:229–240.
12. Wendel DP, Taylor DG, Albertine KH, Keating MT, Li DY. Impaired distal airway development in mice lacking elastin. *Am J Respir Cell Mol Biol* 2000;23:320–326.

13. Neptune ER, Frischmeyer PA, Arking DE, Myers L, Bunton TE, Gayraud B, Ramirez F, Sakai LY, Dietz HC. Dysregulation of TGF-βactivation contributes to pathogenesis in Marfan syndrome. *Nat Genet* 2003;33:407–411.
14. Bostrom H, Willetts K, Pekny M, Leveen P, Lindahl P, Hedstrand H, Pekna M, Hellstrom M, Gebre-Medhin S, Schalling M, *et al.* PDGF-A signaling is a critical event in lung alveolar myofibroblast development and alveogenesis. *Cell* 1996;85:863–873.
15. McGowan S, Jackson SK, Jenkins-Moore M, Dai HH, Chambon P, Snyder JM. Mice bearing deletions of retinoic acid receptors demonstrate reduced lung elastin and alveolar numbers. *Am J Respir Cell Mol Biol* 2000;23:162–167.
16. Powell PP, Wang CC, Horinouchi H, Shepherd K, Jacobson M, Lipson M, Jones R. Differential expression of fibroblast growth factor receptors 1 to 4 and ligand genes in late fetal and early postnatal rat lung. *Am J Respir Cell Mol Biol* 1998;19:563–572.
17. Lopez E, Boucherat O, Franco-Montoya ML, Bourbon JR, Delacourt C, Jarreau PH. Nitric oxide donor restores lung growth factor and receptor expression in hyperoxia-exposed rat pups. *Am J Respir Cell Mol Biol* 2006;34:738–745.
18. Wagenaar GT, ter Horst SA, van Gastelen MA, Leijser LM, Mauad T, van der Velden PA, de Heer E, Hiemstra PS, Poorthuis BJ, Walther FJ. Gene expression profile and histopathology of experimental bronchopulmonary dysplasia induced by prolonged oxidative stress. *Free Radic Biol Med* 2004;36:782–801.
19. Weinstein M, Xu X, Ohyama K, Deng CX. FGFR-3 and FGFR-4 function cooperatively to direct alveogenesis in the murine lung. *Development* 1998;125:3615–3623.
20. Mariani TJ, Reed JJ, Shapiro SD. Expression profiling of the developing mouse lung: insights into the establishment of the extracellular matrix. *Am J Respir Cell Mol Biol* 2002;26:541–548.
21. Mariani TJ, Shapiro SD. Thomas A. Neff lecture: application of expression profiling to the developing lung: identification of putative regulatory networks controlling matrix production. *Chest* 2002;121(3, Suppl)42S–44S.
22. Li X, Chen Y, Scheele S, Arman E, Haffner-Krausz R, Ekblom P, Lonai P. Fibroblast growth factor signaling and basement membrane assembly are connected during epithelial morphogenesis of the embryoid body. *J Cell Biol* 2001;153:811–822.
23. Yamabe H, Osawa H, Kaizuka M, Tsunoda S, Shirato K, Tateyama F, Okumura K. Platelet-derived growth factor, basic fibroblast growth factor, and interferon gamma increase type IV collagen production in human fetal mesangial cells via a transforming growth factor-β–dependent mechanism. *Nephrol Dial Transplant* 2000;15:872–876.
24. Srisuma S, Arikan MC, Simon DM, Mariani TJ. Fibroblast growth factor receptor signaling regulates extracellular matrix gene expression in murine lung cells [abstract]. *FASEB J* 2005;19:A1603–A1604.
25. Srisuma S, Bhattacharya S, Mariani TJ. FGF signaling contributes to the regulation of epithelial cell basement membrane gene expression during alveolar formation [abstract]. *Am J Respir Crit Care Med* 2008; 177:A23.
26. Srisuma S, Bhattacharya S, Tu F, Starcher B, Mariani TJ. Fibroblast growth factor receptor deficiency results in abnormal type II pneumocyte gene expression and dysregulation of matrix production [abstract]. *FASEB J* 2007;21:A10.
27. Colvin JS, Bohne BA, Harding GW, McEwen DG, Ornitz DM. Skeletal overgrowth and deafness in mice lacking fibroblast growth factor receptor 3. *Nat Genet* 1996;12:390–397.
28. Davidson D, Blanc A, Filion D, Wang H, Plut P, Pfeffer G, Buschmann MD, Henderson JE. Fibroblast growth factor (FGF) 18 signals through FGF receptor 3 to promote chondrogenesis. *J Biol Chem* 2005;280:20509–20515.
29. Simon DM, Arikan MC, Srisuma S, Bhattacharya S, Tsai LW, Ingenito EP, Gonzalez F, Shapiro SD, Mariani TJ. Epithelial cell PPAR[gamma] contributes to normal lung maturation. *FASEB J* 2006;20:1507–1509.
30. Soutiere SE, Mitzner W. Comparison of postnatal lung growth and development between C3H/HeJ and C57BL/6J mice. *J Appl Physiol* 2006;100:1577–1583.
31. Bhattacharya S, Srisuma S, Demeo DL, Shapiro SD, Bueno R, Silverman EK, Reilly JJ, Mariani TJ. Molecular biomarkers for quantitative and discrete COPD phenotypes. *Am J Respir Cell Mol Biol* 2009;40:359–367.
32. Li C, Wong WH. Model-based analysis of oligonucleotide arrays: expression index computation and outlier detection. *Proc Natl Acad Sci USA* 2001;98:31–36.
33. Tusher VG, Tibshirani R, Chu G. Significance analysis of microarrays applied to the ionizing radiation response. *Proc Natl Acad Sci USA* 2001;98:5116–5121.
34. Kramer EL, Deutsch GH, Sartor MA, Hardie WD, Ikegami M, Korfhagen TR, Le Cras TD. Perinatal increases in TGF-{alpha} disrupt the saccular phase of lung morphogenesis and cause remodeling: microarray analysis. *Am J Physiol Lung Cell Mol Physiol* 2007; 293:L314–L327.
35. Veness-Meehan KA, Pierce RA, Moats-Staats BM, Stiles AD. Retinoic acid attenuates O2-induced inhibition of lung septation. *Am J Physiol Lung Cell Mol Physiol* 2002;283:L971–L980.
36. Hirakawa H, Pierce RA, Bingol-Karakoc G, Karaaslan C, Weng M, Shi GP, Saad A, Weber E, Mariani TJ, Starcher B, *et al.* Cathepsin S deficiency confers protection from neonatal hyperoxia-induced lung injury. *Am J Respir Crit Care Med* 2007;176:778–785.
37. DeMeo DL, Mariani TJ, Lange C, Srisuma S, Litonjua AA, Celedon JC, Lake SL, Reilly JJ, Chapman HA, Mecham BH, *et al.* The SERPINE2 gene is associated with chronic obstructive pulmonary disease. *Am J Hum Genet* 2006;78:253–264.
38. Kho AT, Bhattacharya S, Mecham BH, Hong J, Kohane IS, Mariani TJ. Expression profiles of the mouse lung identify a molecular signature of time-to-birth. *Am J Respir Cell Mol Biol* 2009;40:47–57.
39. Warshamana GS, Corti M, Brody AR. TNF-α, PDGF, and TGF-β(1) expression by primary mouse bronchiolar-alveolar epithelial and mesenchymal cells: tnf-alpha induces TGF-β(1). *Exp Mol Pathol* 2001;71:13–33.
40. Bhattacharya S, Long D, Lyons-Weiler J. Overcoming confounded controls in the analysis of gene expression data from microarray experiments. *Appl Bioinformatics* 2003;2:197–208.
41. Chailley-Heu B, Boucherat O, Barlier-Mur AM, Bourbon JR. FGF-18 is upregulated in the postnatal rat lung and enhances elastogenesis in myofibroblasts. *Am J Physiol Lung Cell Mol Physiol* 2005;288: L43–L51.
42. Palmon A, Roos H, Reichenberg E, Grosskop A, Bar Kana I, Pitaru S, Redlich M. Basic fibroblast growth factor suppresses tropoelastin gene expression in cultured human periodontal fibroblasts. *J Periodontal Res* 2001;36:65–70.
43. Li C, Hu L, Xiao J, Chen H, Li JT, Bellusci S, Delanghe S, Minoo P. Wnt5a regulates Shh and Fgf10 signaling during lung development. *Dev Biol* 2005;287:86–97.
44. Li J, Hoyle GW. Overexpression of PDGF-A in the lung epithelium of transgenic mice produces a lethal phenotype associated with hyperplasia of mesenchymal cells. *Dev Biol* 2001;239:338–349.
45. Badesch DB, Lee PD, Parks WC, Stenmark KR. Insulin-like growth factor I stimulates elastin synthesis by bovine pulmonary arterial smooth muscle cells. *Biochem Biophys Res Commun* 1989;160:382–387.
46. Davidson JM, Zoia O, Liu JM. Modulation of transforming growth factor-β1 stimulated elastin and collagen production and proliferation in porcine vascular smooth muscle cells and skin fibroblasts by basic fibroblast growth factor, transforming growth factor–α, and insulin-like growth factor–I. *J Cell Physiol* 1993;155:149–156.
47. Foster J, Rich CB, Florini JR. Insulin-like growth factor I, somatomedin C, induces the synthesis of tropoelastin in aortic tissue. *Coll Relat Res* 1987;7:161–169.
48. Rich CB, Goud HD, Bashir M, Rosenbloom J, Foster JA. Developmental regulation of aortic elastin gene expression involves disruption of an IGF-I sensitive repressor complex. *Biochem Biophys Res Commun* 1993;196:1316–1322.
49. Srinivasan S, Strange J, Awonusonu F, Bruce MC. Insulin-like growth factor I receptor is downregulated after alveolarization in an apoptotic fibroblast subset. *Am J Physiol Lung Cell Mol Physiol* 2002;282: L457–L467.
50. Powell-Braxton L, Hollingshead P, Warburton C, Dowd M, Pitts-Meek S, Dalton D, Gillett N, Stewart TA. IGF-I is required for normal embryonic growth in mice. *Genes Dev* 1993;7:2609–2617.
51. Liu JP, Baker J, Perkins AS, Robertson EJ, Efstratiadis A. Mice carrying null mutations of the genes encoding insulin-like growth factor I (Igf-1) and type 1 IGF receptor (Igf1r). *Cell* 1993;75:59–72.
52. Rich CB, Ewton DZ, Martin BM, Florini JR, Bashir M, Rosenbloom J, Foster JA. IGF-I regulation of elastogenesis: comparison of aortic and lung cells. *Am J Physiol* 1992;263:L276–L282.
53. Noguchi A, Nelson T. IGF-I stimulates tropoelastin synthesis in neonatal rat pulmonary fibroblasts. *Pediatr Res* 1991;30:248–251.
54. McGowan SE, McNamer R. Transforming growth factor-β increases elastin production by neonatal rat lung fibroblasts. *Am J Respir Cell Mol Biol* 1990;3:369–376.

55. Liu B, Harvey CS, McGowan SE. Retinoic acid increases elastin in neonatal rat lung fibroblast cultures. *Am J Physiol* 1993;265:L430–L437.
56. Bellusci S, Grindley J, Emoto H, Itoh N, Hogan BL. Fibroblast growth factor 10 (FGF10) and branching morphogenesis in the embryonic mouse lung. *Development* 1997;124:4867–4878.
57. Sutherland D, Samakovlis C, Krasnow MA. branchless encodes a *Drosophila* FGF homolog that controls tracheal cell migration and the pattern of branching. *Cell* 1996;87:1091–1101.
58. Suga T, Kurabayashi M, Sando Y, Ohyama Y, Maeno T, Maeno Y, Aizawa H, Matsumura Y, Kuwaki T, Kuro OM, *et al.* Disruption of the klotho gene causes pulmonary emphysema in mice: defect in maintenance of pulmonary integrity during postnatal life. *Am J Respir Cell Mol Biol* 2000;22:26–33.
59. Razzaque MS, Sitara D, Taguchi T, St-Arnaud R, Lanske B. Premature aging–like phenotype in fibroblast growth factor 23 null mice is a vitamin D–mediated process. *FASEB J* 2006;20:720–722.
60. Mandeville I, Aubin J, LeBlanc M, Lalancette-Hebert M, Janelle MF, Tremblay GM, Jeannotte L. Impact of the loss of Hoxa5 function on lung alveogenesis. *Am J Pathol* 2006;169:1312–1327.
61. Hokuto I, Perl AK, Whitsett JA. Prenatal, but not postnatal, inhibition of fibroblast growth factor receptor signaling causes emphysema. *J Biol Chem* 2003;278:415–421.
62. Perl AK, Gale E. FGF Signaling is required for myofibroblast differentiation during alveolar regeneration. *Am J Physiol Lung Cell Mol Physiol* 2009;297:L299–L309.
63. Cool SM, Sayer RE, van Heumen WR, Pickles JO, Nurcombe V. Temporal and spatial expression of fibroblast growth factor receptor 4 isoforms in murine tissues. *Histochem J* 2002;34:291–297.
64. Liu X, Zhao Y, Gao J, Pawlyk B, Starcher B, Spencer JA, Yanagisawa H, Zuo J, Li T. Elastic fiber homeostasis requires lysyl oxidase–like 1 protein. *Nat Genet* 2004;36:178–182.
65. McLaughlin PJ, Chen Q, Horiguchi M, Starcher BC, Stanton JB, Broekelmann TJ, Marmorstein AD, McKay B, Mecham R, Nakamura T, *et al.* Targeted disruption of fibulin-4 abolishes elastogenesis and causes perinatal lethality in mice. *Mol Cell Biol* 2006;26:1700–1709.
66. Thibeault DW, Mabry SM, Ekekezie II, Truog WE. Lung elastic tissue maturation and perturbations during the evolution of chronic lung disease. *Pediatrics* 2000;106:1452–1459.
67. Alejandre-Alcazar MA, Kwapiszewska G, Reiss I, Amarie OV, Marsh LM, Sevilla-Perez J, Wygrecka M, Eul B, Kobrich S, Hesse M, *et al.* Hyperoxia modulates TGF-β/BMP signaling in a mouse model of bronchopulmonary dysplasia. *Am J Physiol Lung Cell Mol Physiol* 2007;292:L537–L549.
68. Bland RD, Xu L, Ertsey R, Rabinovitch M, Albertine KH, Wynn KA, Kumar VH, Ryan RM, Swartz DD, Csiszar K, *et al.* Dysregulation of pulmonary elastin synthesis and assembly in preterm lambs with chronic lung disease. *Am J Physiol Lung Cell Mol Physiol* 2007;292: L1370–L1384.
69. Coalson JJ, Winter VT, Siler-Khodr T, Yoder BA. Neonatal chronic lung disease in extremely immature baboons. *Am J Respir Crit Care Med* 1999;160:1333–1346.
70. McCurnin DC, Pierce RA, Chang LY, Gibson LL, Osborne-Lawrence S, Yoder BA, Kerecman JD, Albertine KH, Winter VT, Coalson JJ, *et al.* Inhaled NO improves early pulmonary function and modifies lung growth and elastin deposition in a baboon model of neonatal chronic lung disease. *Am J Physiol Lung Cell Mol Physiol* 2005;288: L450–L459.
71. Park MS, Rieger-Fackeldey E, Schanbacher BL, Cook AC, Bauer JA, Rogers LK, Hansen TN, Welty SE, Smith CV. Altered expressions of fibroblast growth factor receptors and alveolarization in neonatal mice exposed to 85% oxygen. *Pediatr Res* 2007;62:652–657.
72. McGowan SE, Jackson SK, Olson PJ, Parekh T, Gold LI. Exogenous and endogenous transforming growth factors-βinfluence elastin gene expression in cultured lung fibroblasts. *Am J Respir Cell Mol Biol* 1997;17:25–35.
73. Conn KJ, Rich CB, Jensen DE, Fontanilla MR, Bashir MM, Rosenbloom J, Foster JA. Insulin-like growth factor–I regulates transcription of the elastin gene through a putative retinoblastoma control element: a role for Sp3 acting as a repressor of elastin gene transcription. *J Biol Chem* 1996;271:28853–28860.
74. Trackman PC, Graham RJ, Bittner HK, Carnes DL, Gilles JA, Graves DT. Inflammation-associated lysyl oxidase protein expression in vivo, and modulation by FGF-2 plus IGF-1. *Histochem Cell Biol* 1998;110: 9–14.
75. Noguchi A, Samaha H. Developmental changes in tropoelastin gene expression in the rat lung studied by *in situ* hybridization. *Am J Respir Cell Mol Biol* 1991;5:571–578.
76. Florin L, Maas-Szabowski N, Werner S, Szabowski A, Angel P. Increased keratinocyte proliferation by JUN-dependent expression of PTN and SDF-1 in fibroblasts. *J Cell Sci* 2005;118:1981–1989.
77. Guo Y, Graham-Evans B, Broxmeyer HE. Murine embryonic stem cells secrete cytokines/growth modulators that enhance cell survival/anti-apoptosis and stimulate colony formation of murine hematopoietic progenitor cells. *Stem Cells* 2006;24:850–856.
78. Onoue T, Uchida D, Begum NM, Tomizuka Y, Yoshida H, Sato M. Epithelial–mesenchymal transition induced by the stromal cell–derived factor-1/CXCR4 system in oral squamous cell carcinoma cells. *Int J Oncol* 2006;29:1133–1138.
79. Nakayama T, Mutsuga N, Tosato G. Effect of fibroblast growth factor 2 on stromal cell–derived factor 1 production by bone marrow stromal cells and hematopoiesis. *J Natl Cancer Inst* 2007;99:223–235.
80. Nakayama T, Mutsuga N, Tosato G. FGF2 posttranscriptionally down-regulates expression of SDF1 in bone marrow stromal cells through FGFR1 IIIc. *Blood* 2007;109:1363–1372.